Derivation of Force Field Parameters for SnO_2−H_2O Surface Systems from Plane-Wave Density Functional Theory Calculations

A. V. Bandura,[†] J. O. Sofo,[‡] and J. D. Kubicki*[,§]

St. Petersburg State University, St. Petersburg, Russia, and Department of Physics and Department of Geosciences and the Earth & Environmental Systems Institute, The Pennsylvania State University, University Park, Pennsylvania 16802

Received: May 5, 2005; In Final Form: February 27, 2006

Plane-wave density functional theory (DFT-PW) calculations were performed on bulk SnO_2 (cassiterite) and the (100), (110), (001), and (101) surfaces with and without H_2O present. A classical interatomic force field has been developed to describe bulk SnO_2 and SnO_2−H_2O surface interactions. Periodic density functional theory calculations using the program VASP (Kresse et al., 1996) and molecular cluster calculations using Gaussian 03 (Frisch et al., 2003) were used to derive the parametrization of the force field. The program GULP (Gale, 1997) was used to optimize parameters to reproduce experimental and ab initio results. The experimental crystal structure and elastic constants of SnO_2 are reproduced reasonably well with the force field. Furthermore, surface atom relaxations and structures of adsorbed H_2O molecules agree well between the ab initio and force field predictions. H_2O addition above that required to form a monolayer results in consistent structures between the DFT-PW and classical force field results as well.

Introduction

Adsorption of metal ions to oxide surfaces is an important phenomenon in the fate, transport, and bioavailability of contaminants in the environment.[1] One factor that affects adsorption of metals to oxide surfaces is the so-called electrical double layer that is thought to develop near the interface between water and charged surfaces. However, this nanoscale domain (1−2 nm) is not well understood in terms of atomic structure and physical properties because it is difficult to separate from the bulk fluid and solid behavior. A major aim of research on this topic is to assess the atomic structure of the oxide−water interface and obtain information on how this region differs from bulk properties. Initial work in a collaborative effort to observe and model oxide−water interfaces has focused on the model system α-TiO_2.[2−5] The successful merging of potentiometry, spectroscopy, diffractrometry, and molecular and thermodynamic modeling has led us to explore other systems in order to understand how the properties of bulk materials influence the oxide−water interface.

In contrast to TiO_2, the mineral SnO_2 (cassiterite) was selected because it has the same crystal structure as α-TiO_2 but a much lower dielectric constant (9 vs 121). Sverjensky[6] has theorized that the bulk crystal and interfacial dielectric constants play a dominant role in controlling whether dehydrated ions adsorb directly onto the oxide surface or form electrostatically adsorbed outer-sphere complexes. Development of a classical interatomic force field for SnO_2−H_2O using the same methods employed in the development of our earlier force field for α-TiO_2[7] will allow for molecular dynamics (MD) simulations (see ref 8 for MD simulation results on α-TiO_2−H_2O.) that can model the oxide−water interface for comparison of water structure and ion adsorption behavior in a self-consistent manner.

Ab initio modeling studies contrasting the adsorption of H_2O on SnO_2 and TiO_2 have been previously conducted by Goniakowski and Gillan[9] and Lindan.[10] The latter authors predicted significant differences in the structure of adsorbed H_2O on these surfaces where dissociative adsorption (i.e., H_2O + ≡SnO + ≡Sn → 2 ≡SnOH, where ≡ denotes the atom is a surface site) was favored on SnO_2 vs associative adsorption (i.e., H_2O + ≡Ti → ≡$TiOH_2$) on TiO_2. Lindan[10] attributed the difference in H_2O behavior on the surface to the larger unit cell parameters of SnO_2 compared to TiO_2 ($a = b = 4.737$ Å; $c = 3.186$ Å vs $a = b = 4.594$ Å; $c = 2.959$ Å, respectively). Larger cell dimensions caused H-bonding among H_2O molecules on the surface to be less energetically important on SnO_2 than on TiO_2. Other studies using ab initio methods[11] arrived at similar conclusions. Ab initio calculations presented here are consistent with Lindan,[10] and the results are used to develop an interatomic force field to describe larger SnO_2−H_2O model systems.

Our previous study of α-TiO_2[7] revised the force field of Matsui and Akaogi[12] to include terms for the underbonded Ti and O surface atoms as well as parameters for Ti, O, and H_2O interaction. This parametrization and surface structure were then fed into MD simulations conducted by Předota et al.[8] A similar procedure was adopted here except that a preexisting force field for SnO_2 was not used as the basis for the SnO_2−H_2O force field. Although bulk SnO_2 force fields exist,[13−17] most of them use the formal ion charges and introduce the oxygen polarizability via the shell model of Dick and Overhauser.[18] However, the shell model may not be wholly consistent with the SPC/E model[19] of water. Consequently, ab initio calculations were conducted on bulk SnO_2 to derive a force field parametrization based on the same terms as found in Bandura and Kubicki.[7]

Method

1. General Approach. The force field was based on the simple forms of additive atom−atom potentials including

[†] St. Petersburg State University.
[‡] Department of Physics, The Pennsylvania State University.
[§] Department of Geosciences and the Earth & Environmental Systems Institute, The Pennsylvania State University.

10.1021/jp0523423 CCC: $33.50
Published on Web 04/04/2006

TABLE 1: Calculated Atomic Charges for H_2O and $Sn(OH)_4$ Molecules and for Solid SnO_2

substance	atom	core charge, *e*	VASP[a] electronic charge, *e*	scaled electronic charge, *e*	calculated atomic charge, *e*	reference[b] charge, *e*
H_2O	O	6	6.980	6.8364	−0.836	−0.8476
	H	1	0.594	0.5818	0.418	0.4238
	sum:	8	8.168	8	0	0
$Sn(OH)_4$	Sn	14	12.027	12.024	1.976	2.012
	O	6	6.909	6.908	−0.908	−0.944
	H	1	0.586	0.586	0.414	0.441
	sum:	42	42.007	42	0	0
SnO_2[c]	Sn	14	11.979	11.95	2.050	
	O	6	7.042[d]	7.025	−1.025	
	sum:	26	26.063	26	0	

[a] VASP optimized geometry, 10 × 10 × 10 Å cell; $R_{WIGS}(Sn) = 1.42$ Å; $R_{WIGS}(O) = 1.35$ Å; $R_{WIGS}(H) = 0.56$ Å. [b] SPC/E (ref 19) charges for water and CHelpG (ref 28) charges for $Sn(OH)_4$ using HF result with VASP optimized geometry. [c] Experimental (ref 25) geometry: $a = 4.737$, $b = 4.737$, and $c = 3.186$ Å. [d] Averaged electronic charge on oxygen.

electrostatic and short-range terms. Three forms were used for short-range interactions: Buckingham, harmonic, and Lennard-Jones. Angle-bending terms were also included to model the Sn−O−H and H−O−H interactions. A previously derived[7] procedure for determination of the parameter values for TiO_2-H_2O was used. The force field was built for compatibility with the SPC/E model for H_2O-H_2O interactions.[19] The main difference between the TiO_2-H_2O force field[7] and the present one is that the bulk properties of SnO_2 as well as bare surfaces with the low crystallographic indexes have been included in the fitting process from the beginning. Another distinction is the method for extracting the effective atomic charges to be used in Coulomb terms. A direct procedure was adopted for calculating charges on all atoms based on the results of the charge density integration within the Wigner−Seitz spheres calculated with the VASP[20] package.

2. Computational Details. The VASP[20,21] package has been used to perform the all plane-wave density functional theory (DFT-PW) calculations of SnO_2, $Sn(OH)_4$ and SnO_2-H_2O systems needed for developing the force field. Projector-augmented-wave (PAW) pseudopotentials[22,23] were used for core-valence electron interactions and the PBE form[24] of GGA was adopted for the exchange-correlation functionals. Medium-range values of the energy cutoff, ENCUT = 400 eV, cutoff for the augmentation charges, and sufficiently large number NG_i and NG_iF of grid points for the fast Fourier transformations (in the case of bulk crystal: NGX = NGY = 32, NGZ = 24; $NG_iF = 2NG_i$, i = X, Y, Z) have been applied in all calculations. The PAW pseudopotential for tin atoms with default energy cutoff ENMAX = 241 eV, which explicitly treats 4d electrons as valence, has been used. Geometry optimizations were carried out until all forces on atoms were less than 0.01 eV/Å. The constrained experimental crystal structure[25] was used for bulk SnO_2 calculations: $a = b = 4.737$ Å; $c = 3.186$ Å; $u = 0.306$ (space group $P4_2/mnm$), Γ-centered Monkhorst−Pack[26] 4 × 4 × 6 grids has been used for the Brillouin zone sampling in bulk crystal calculations. For slab calculations, the number of *k*-points was decreased proportionally corresponding to the reduction of the Brillouin zone.

Sn−hydroxide molecules were used to approximate Sn−OH surface groups on SnO_2 surfaces. Gaussian 03[27] was used for obtaining the CHelpG[28] charges on atoms in the small Sn−hydroxide complexes and for calculating the vibrational frequencies of $Sn(OH)_4$. The CHelpG method for obtaining charges was chosen because we are most interested in reproducing the electrostatic properties of the SnO_2-H_2O interface. The standard Gaussian basis set 6-311+G(d,p) was used for H and O atoms in these calculations. For Sn atoms, the aug_cc-pVTZ[29] pseudopotentials and corresponding basis set were used, which is comparable with the 6-311+G(d,p) in quality. The CHelpG charges were estimated using Hartree−Fock (HF) approximation, and the DFT-B3LYP method was used for the frequency calculations.

3. Estimation of Atomic Charges. Coulombic terms introduce the major contribution to the intra- and intermolecular interactions in this force field. For this reason, the values of atomic charges must be determined accurately before all other parameters. Atomic charges are not physical observables, so some additional assumptions are needed for obtaining reliable values. In the VASP package, the wave function character is calculated by projecting the wave functions onto spherical harmonics that are nonzero within spheres of a radius R_{WIGS} around each ion, and the integrated electronic charge within R_{WIGS} is then calculated. The charges produced in this manner, however, are dependent on the value of R_{WIGS}, and their sums generally do not coincide with the total number of electrons explicitly involved in calculation. Moreover, due to overlapping of Wigner−Seitz spheres some electronic charge is accounted for twice. Nevertheless, we found that when the surface systems were calculated, the relative changes in atomic charges reasonably reproduced the expected deviations. Thus, calculated charges on 6-fold and 5-fold Sn do not differ considerably, whereas the charges on bridging oxygens are noticeably less negative than their bulk values in the case of the bare relaxed surfaces in agreement with our previous ab initio results for TiO_2.[4] Oxygen and hydrogen charges for the hydroxyl groups were arranged in order: $|q(O_{br})| > |q(O_{term})|$ and $q(H_{br}) > q(H_{term})$, which is correlated with the acidity of the corresponding hydroxyl groups on typical oxide surfaces.[30] Also, what may be more important, the application of VASP charges in preliminary versions of the force field qualitatively reproduced the correct relaxations of the atomic positions on the surface compared to ab initio structures (see Results).

We adopted the following semiempirical scheme for extracting the charges from VASP results:

1. Choose R_{WIGS} for O and H atoms so that charges calculated by VASP[20,21] for an isolated water molecule were approximately equal to the atomic charges in the SPC water model (see Table 1). The resulting values are $R_{WIGS}(H) = 0.56$ and $R_{WIGS}(O) = 1.35$ Å. (Note: H_2O was placed in a periodic box of 10 × 10 × 10 Å to find the values for R_{WIGS}.)

2. Chose the R_{WIGS} for Sn atoms such that VASP results for the charge on the Sn atoms in small hydroxide complexes was approximately equal to the Sn charge obtained by CHelpG[28] method using Gaussian 03[27] calculations of the same complexes (see Table 1). The resulting value is 1.42 Å.

3. Scale the electronic charge produced by VASP on all atoms such that the total sum of charges would be equal to the total

TABLE 2: Parameters of 3D Periodic Slab Models of SnO_2

face index	*a*, Å	*b*, Å	*c*, Å	applied space group	*k*-point set	vacuum gap, Å	no. of atomic planes/Sn_2O_4 layers	ab initio surface energy, J m^{-2}	
								this work	ref 31
110	3.186	6.700	20.099	*Pmmm*	$6 \times 3 \times 1$	10.813	9/3	1.01[a]	1.04
100	3.186	4.737	23.686	*P*2/*m*	$6 \times 4 \times 1$	12.383	15/2.5	0.92	1.14
001	4.737	4.737	15.932	*C*222	$4 \times 4 \times 1$	9.559	5/2.5	1.74	1.72
101	4.737	5.709	15.864	$P\bar{1}$	$4 \times 3 \times 1$	8.952	9/3	1.28	1.33

[a] For the thicker slabs of the (110) surface we have obtained 0.91 and 0.85 J m^{-2} for the five and seven Sn_2O_4 layer slabs, respectively.

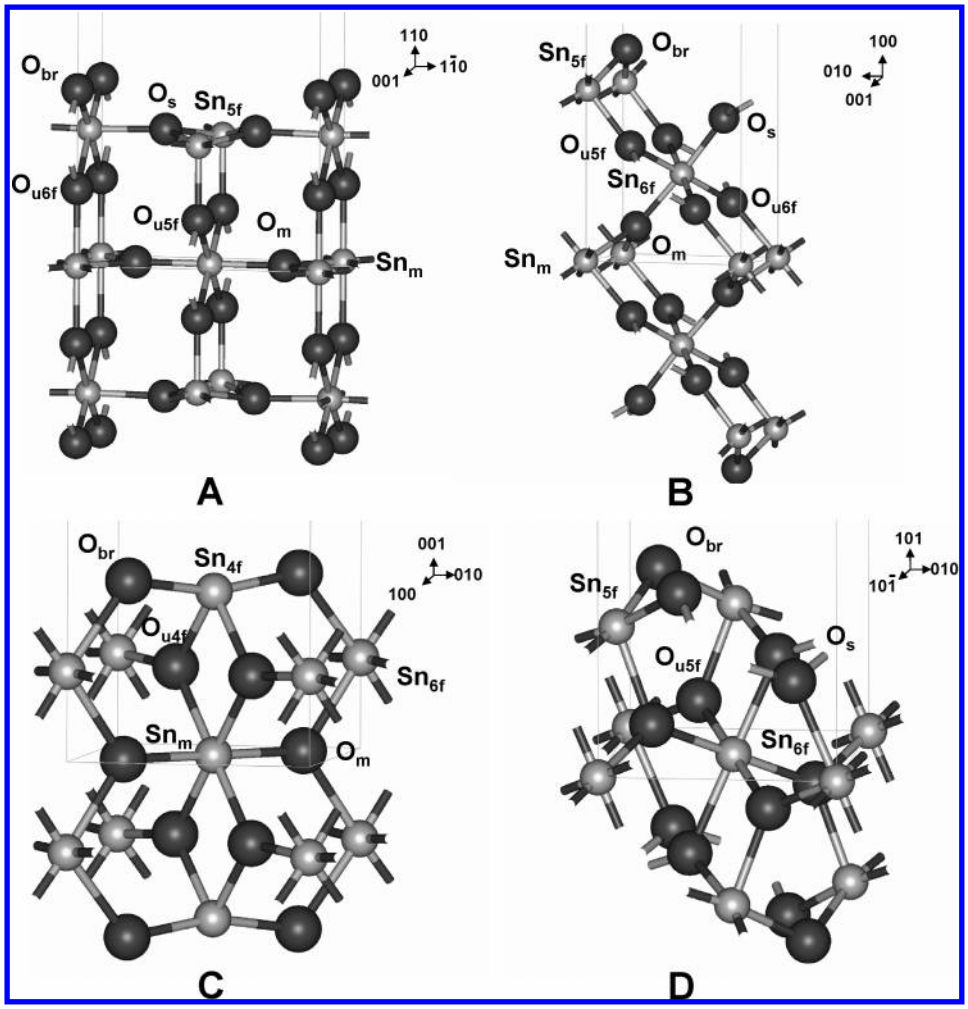

Figure 1. Relaxed structure of the model slab systems for SnO_2 surface with the low crystallographic indexes calculated by VASP: A, (110) face; B, (100) face; C, (001) face; D, (101) face. Corresponding structural parameters are given in Tables 2−6.

number of electrons in the system. Final atomic charges were calculated as the core charge minus scaled electronic charge for every atom.

4. When the neutral (associated) H_2O molecules are present in the system, the electronic charge of water atoms and corresponding number of electrons should be subtracted before scaling. The reason of this is that charges on atoms in H_2O are defined in the SPC/E[19] model.

The advantage of the procedure described above is that it can provide the atomic charges for any neutral or charged system of moderate size. The charges obtained for the bulk crystal atoms are given in Table 1.

Results

1. Relaxation of (110), (100), (001), and (101) Faces of SnO_2. The relaxation of low-index faces of SnO_2 with the rutile structure has been investigated by Oviedo and Gillan.[31] Nevertheless, we made our own DFT calculation of the relaxed surfaces to provide data for force field deviation and to verify that we were performing these calculations correctly. We did not intend to investigate the relaxation per se but only to gather the atomic coordinates and charges which can be used in the fitting procedure. For this reason, we did not optimize the bulk crystal geometry. All slab calculations were performed with cell parameters in surface planes fixed to the experimental values. The symmetry restrictions have been applied according to the corresponding space group (see Table 2). The atomic positions of atoms in the central layer also were fixed at the bulk crystal geometry. The characteristics of the slab models are given in Table 2 for all faces investigated (see Figure 1). In the last two columns of Table 2 we compare surface energies obtained by us and by Oviedo and Gillan.[31] The agreement between them is good except a relative order for (110) and (100) surfaces. This jump is due to the comparatively small number of Sn_2O_4

TABLE 3: Relaxation of the SnO_2 (110) Surface (Å) and Charges on Atoms Obtained by VASP Calculations (Three Sn-Layer Slab Results)

atom	*z*-coordinate in bulk geometry	*z*-shift, VASP	*z*-shift, force field	*z*-shift, ref 31	VASP atomic charges, *e*
Sn_{6f}, 6-fold surface tin	3.350	0.24	0.24	0.22	1.991
Sn_{5f}, 5-fold surface tin	3.350	0.01	0.01	−0.11	1.992
Sn_m, 6-fold tin in the middle layer	0.000				1.991
O_{br}, bridging oxygen	4.643	0.16	0.22	0.09	−0.871
O_s, 3-fold surface oxygen	3.350	0.28	0.21	0.18	−1.03
O_{u6f}, sub-bridging oxygen	2.057	0.05	0.11	0.07	−0.903
O_{u5f}, oxygen underneath Sn_{5f}	1.293	0.04	0.06	−0.04	−1.063
O_m, oxygen in the middle layer	0.000				−1.077

TABLE 4: Relaxation of the SnO_2 (100) Surface (Å) and Charges on Atoms Obtained by VASP Calculations (Five Sn-Layer Slab Results)

atom	*z*-coordinate in bulk geometry	*z*-shift, VASP	*z*-shift, force field	*z*-shift, ref 31	VASP atomic charges, *e*
Sn_{5f}, surface 5-fold tin	4.737	0.22	0.12	0.05	1.993
Sn_{6f}, surface 6-fold tin	2.369	0.10	0.05		1.969
Sn_m, 6-fold tin in the middle layer	0.000				1.978
O_{br}, bridging oxygen	5.652	0.37	0.31	0.18	−0.835
O_s, 3-fold surface oxygen	3.823	0.29	0.27	0.09	−0.967
O_{u5f}, oxygen underneath Sn_{5f}	3.283	0.07	0.13		−1.057
O_{u6f}, oxygen underneath Sn_{6f}	1.454	0.11	0.14		−1.046
O_m, oxygen in the middle layer	0.914	0.00	−0.01		−1.046

TABLE 5: Relaxation of the SnO_2 (001) Surface (Å) and Charges on Atoms Obtained by VASP Calculations (Five Sn-Layer Slab Results)

atom	*z*-coordinate in bulk geometry	*z*-shift, VASP	*z*-shift, force field	*z*-shift, ref 31	VASP atomic charges, *e*
Sn_{4f}, surface 4-fold tin	3.186	−0.05	0.00	−0.16	1.876
Sn_{6f}, surface 6-fold tin	1.593	0.14	0.07	0.17	2.035
Sn_m, 6-fold tin in the middle layer	0.000				1.912
O_{br}, bridging oxygen	3.186	0.23	0.23	0.16	−0.791
O_{u4f}, 3-fold oxygen underneath Sn_{4f}	1.593	0.01	0.08	−0.04	−1.142
O_m, oxygen[a] in the middle layer	0.000				−1.001

[a] This oxygen was allowed to relax in the *xy* plane.

TABLE 6: Relaxation of the SnO_2 (101) Surface (Å) and Charges on Atoms Obtained by VASP Calculations (Three Sn-Layer Slab Results)

atom	*z*-coordinate in bulk geometry	*z*-shift, VASP	*z*-shift, force field	*z*-shift, ref 31	VASP atomic charges, *e*
Sn_{5f}, 5-fold surface tin	2.644	0.06	0.04	0.01	1.978
Sn_{6f}, 6-fold tin in the middle layer	0.000				1.928
O_{br}, bridging oxygen	3.456	0.15	0.13	0.09	−0.878
O_s, 3-fold surface oxygen	1.832	0.15	0.21	0.11	−0.936
O_{u5f}, oxygen underneath Sn_{5f}	0.812	−0.05	0.01	0.04	−1.129

layers used in the slabs for our force field deviation (i.e., 2.5−3 in our calculations and 5−6 in the Oviedo and Gillan[31] study). Thus, for the 5 and 7 Sn_2O_4-layer slabs of (110) surface, we have obtained the values of 0.91 and 0.85 J m^{-2}, correspondingly, which is noticeably lower than that for the 3 Sn_2O_4-layer slab, 1.01 J m^{-2}. In general, solids with lower dielectric constants, such as SnO_2, are expected to have their long-range electrostatic interactions decay more slowly.

In Tables 3−6, we present the vertical displacements of atoms for different surfaces and compare them with the results of Oviedo and Gillan[31] obtained via VASP[20] calculations of thicker slabs using GGA-PW91[32] and ultrasoft potentials[33] with 396 eV cutoff. The charges calculated by the method described above are also included in these tables, as well as the force field results discussed below.

In general, the force field results for atomic relaxation in the *z*-direction relative to each surface were consistent with the results predicted by using VASP in this study. There is also good agreement (within approximately 0.1 Å) with the calculations of Oviedo and Gillan[31] for most atoms. A few exceptions exist: 5-fold Sn on the (110) surface (Table 3), and bridging 3-fold O on the (100) surface (Table 4). Because the ab initio calculations in both studies are based on similar methods in the program VASP,[20] the differences must be due to differences in selected parameters such as the energy cutoff (396 eV in Oviedo and Gillan versus 400 eV here), *k*-point sampling ($3 \times 3 \times 1$ Monkhorst-Pack scheme versus $6 \times 3 \times 1$, $6 \times 4 \times 1$, $4 \times 4 \times 1$, and $4 \times 3 \times 1$ used here), symmetry constrains (Table 2), and vacuum gap (7.5 Å vs ≈9−12 Å used here). The values used here should make the present results somewhat more accurate, but in any case, the differences are relatively insignificant.

2. Determination of Force Field Parameters for Solid-Phase Interactions. Simultaneous empirical fitting with the "RELAX" keyword within the Generalized Utility Lattice Program (GULP)[34] was applied to obtain the values of potential parameters for Sn−Sn, Sn−O, and O−O interactions in bulk and surface crystal systems. In the fitting procedure, we used the experimental structure for bulk crystal and the calculated geometry of two slab models with indices (100) and (001).

TABLE 7: Cell Parameters, Elastic Constants c_{ij}, and Bulk Modulus K of SnO_2 Crystal

quantity	VASP[a]	force field	experiment (refs 25, 35)
		Cell Parameters	
a, Å	4.829	4.786	4.737
c, Å	3.242	3.286	3.186
u[b]	0.306	0.305	0.306
		Elastic Constants, GPa	
c_{11}	211	247.7	261.7
c_{33}	376	442.3	449.6
c_{44}	100	106.1	103.1
c_{66}	178	187.3	207.4
c_{23}	128	120.8	155.5
c_{12}	142	188.3	177.2
		Bulk Modulus, GPa	
K[c]	177	195.4	212.3

[a] Optimized cell parameters using the VASP potentials with a higher energy cutoff (600 eV) than used in most of our calculations. Elastic constants and bulk modulus have been obtained by fitting the total energy to polynomial of the 4th order in the strain components. [b] Internal parameter for O position. [c] Bulk modulus was not explicitly included in fitting.

TABLE 8: Comparison of the Mode Frequencies (cm^{-1}) at the Γ Point for SnO_2

mode	force field	DFT-LDA (ref 38)	experiment (refs 39, 40)
A_{1g}	631	638	638
A_{2g}	482	366	
B_{1g}	133	105	121
B_{2g}	783	762	782
E_g	429	470	476
$B_{1u}^{(1)}$	161	147	
$B_{1u}^{(2)}$	532	585	
A_{2u}	436	461	477
$E_u^{(1)}$	229	242	244
$E_u^{(2)}$	326	286	293
$E_u^{(3)}$	607	615	618

Second derivative information for the bulk crystal potential was also included via the experimental[35] elastic constants.

Short-range pair interactions have been represented by a Buckingham potential with a cutoff radius of 15 Å. For Sn−O bonds, the dispersion coefficients C_{ij} in Buckingham potential were estimated theoretically using the approach of Fowler et al.[36] from the ionic polarizabilities, taken from ref 37. In Table 7 we compare the experimental bulk crystal properties and those calculated with the final row of parameters. There we also place the VASP results for elastic constants, bulk modulus, and equilibrium geometry of SnO_2 obtained using the higher energy cutoff (600 eV). The phonon frequencies in Γ point of Brillouin zone obtained using our force field are compared with the DFT results of Parlinskia and Kawazoe[38] and the available experimental data[39,40] in Table 8. The vibrations are important for showing accuracy of the force field and for calculating thermodynamic properties. The agreement between the force-field results and literature data is excellent (especially taking into account that bulk frequencies were not included in the fitting procedure). The complete set of the empirical parameters for the developed force field is included in Table 9.

In Tables 3−6, the ab initio and force field structural relaxations are compared to the considered SnO_2 faces. Each relaxed surface structure obtained with the force field is in qualitative agreement with the ab initio results. Furthermore, in most instances, the discrepancy between ab initio and force field results is 0.05 Å or less. We consider this to be reasonable agreement for this force field parametrization although refinements to improve accuracy are certainly possible. For example, additional terms can be included in the pair potential. Thus, a complementary Morse potential for the bonding interaction of Sn−O can significantly improve the agreement between experimental and bulk properties. However, as we found, introducing extra terms can complicate the description of the nonbonding interactions, in particular, the H bonds. As a result, a noticeable improvement of representation of the interactions both within the solid phase and on the surface boundary requires considerably increasing the number of empirical parameters and may reduce their transferability. For this reason, we use the simple Buckingham potentials with the same parameters for Sn−Sn, Sn−O, and O−O interactions (except atomic charges) in all systems considered below.

TABLE 9: Force Field Parameters

Buckingham: $E_{ij} = B_{ij}\exp(-r_{ij}/\rho_{ij}) - C_{ij}/r_{ij}^6$

	B_{ij}, kJ/mol	ρ_{ij}, Å	C_{ij}, kJ/mol Å^6
Sn−Sn	90547100	0.205	608
Sn−O	10364150	0.169	1544
O−O	465467	0.273	4699

Harmonic Bond Stretching: $E_{ij} = K2_{ij}/2(r_{ij} - R_{ij})^2$

	$K2_{ij}$, kJ/mol Å^{-2}	R_{ij}, Å
H−O(Sn)[a]	4876	0.970
H−O_{water}[a]	4701	1.000

Harmonic Angle Bending: $E_{kij} = K2_{kij}/2(\phi_{kij} - \Phi_{kij})^2$

	$K2_{kij}$, kJ/mol rad^{-2}	Φ_{kij}, deg
H−O−H[a]	431.1	109.47
Sn−O−H	127.3	86.90

Lennard-Jones: $E_{ij} = A_{ij}/r_{ij}^{12} - C_{ij}/r_{ij}^6$

	A_{ij}, kJ/mol Å^{12}	C_{ij}, kJ/mol Å^6
Sn−O_{water}	600451	1167
O−O_{water}	1978673	3502
(H)O_h[b]−O_{water}	2561695	3502
O_{water}−O_{water} [19]	2634130	2617

[a] Coulomb interactions between participating atoms are excluded. [b] For the protonated (terminal or bridging) oxygens.

3. Determination of Force Field Parameters for Sn−O−H Stretching and Angle-Bending Terms. In the case of bonded OH groups with neighboring atoms on a SnO_2 surface, a simple two-body central-force potential is not valid. This problem was solved by taking an approach that worked previously with the TiO_2−H_2O force field.[7] Bond-stretching and angle-bending terms were added to model the interactions of the involved atoms. Such equilibrium properties as bond lengths, bond angles, and vibrational frequencies of O−H in hydroxides can be well described by harmonic approximation. Moreover, harmonic potentials are more reliable for classical molecular dynamic simulations than, for example, Morse potentials (which were used previously by us in ref 7). The latter in some cases may lead to the artificial break of O−H bonds if no additional restrictions are imposed on the interatomic distances. Harmonic terms also would make it easier to include the specific force field presented here into more general ones. Therefore, for the O−H bond-stretching and Sn−O−H angle-bending terms, the harmonic approximation was chosen in our work. Further, the Coulomb interactions between the Sn and H atoms bonded to common O atom are strong. These next-nearest-neighbor Coulomb interactions are usually omitted in most molecular mechanics force fields but must be included here because the force field is based on an ionic model of the solid.

TABLE 10: Calculated Bond Distances (*d*, Å) and Angles (deg) in $Sn(OH)_4$

parameter	MP2[a]	B3LYP[a]	VASP	force field
d(SnO)	1.95	1.97	1.98	2.01
d(OH)	0.96	0.96	0.98	0.99
∠SnOH	111.2	112.3	110.6	113.1
∠SnOSn, I[b]	105.6	106.0	105.8	102.9
∠SnOSn, II[b]	117.5	116.7	117.1	123.7

[a] Gaussian 03[27] calculations using aug-cc-pVTZ basis set for Sn and 6-311+G(d,p) basis set for H and O atoms. [b] Two smaller (I) and one large (II) angle adjoins to each SnO bond.

TABLE 11: Harmonic Frequencies of $Sn(OH)_4$ (cm^{-1})

MP2[a]	B3LYP[a]	force field
Sn−O Bond Stretching Vibrations[b]		
629.6	597.5	552.3
649.1	618.4	558.7
664.1	631.3	589.8
664.1	631.3	590.2
Sn−O−H Angle-Bending Vibrations		
859.1	851.0	843.0
878.8	867.3	846.9
881.9	871.9	847.1
881.9	871.9	861.9
O−H Bond Stretching Vibrations		
3869	3838	3816
3869	3838	3817
3870	3838	3818
3872	3840	3818

[a] Gaussian 03[27] calculations using aug-cc-pVTZ basis set for Sn and 6-311+G(d,p) basis set for H and O atoms. [b] Stretching vibrations were not included in the fitting procedure.

To obtain the corresponding force constants, quantum mechanical calculations on a model Sn−hydroxide ($Sn(OH)_4$) complex were performed. The geometrical structure of this system was optimized using VASP and sufficiently large three-dimensional (3D) simulation cells ($x = y = z = 10$ Å). Resulting geometry was used in Gaussian 03[27] calculations to obtain the charges from the Hartree−Fock electron density using the CHelpG[28] method (see Table 1). This method produces the charges fit to the electrostatic potential at points selected sufficiently far away from the atomic cores. The default CHelpG core radii for each element have been used in fitting potentials except the value for Sn which was adopted to be 1.5 Å. The dependence of the LCAO results on the basis set on Sn atom was checked using the different basis sets: LANL2DZ,[41,42] SDB-aug-cc-pVTZ,[43] and aug_cc-pVTZ.[29] Significant differences in CHelpG charges obtained by these basis sets were not observed, but we have chosen the last one as the most extended. For H and O atoms we used the standard 6-311+G(d,p) basis for compatibility with our previous results[7] on TiOH systems. Due to the same reason, the HF electron density was used for the CHelpG analysis. Reoptimization of Sn−hydroxide structures using B3LYP[44,45] and MP2 methods in Gaussian 03[27] produced approximately the geometry obtained by VASP (See Table 10). This permits us to calculate the vibrational frequencies in $Sn(OH)_4$ using both of these methods. Results are presented in Table 11.

The force constants *K*2 both for the two- and three-body harmonic potentials, bond parameter *R*, and angle parameter Φ given in Table 9 were adjusted to reproduce the structure and vibrational frequencies for $Sn(OH)_4$ obtained by B3LYP calculations (see Table 11). The frequencies of Sn−O−H bending vibrations have been included explicitly as well as the equilibrium atomic positions in empirical fitting procedure using GULP[34] program. Taking into account the applicability of the force field to be derived, the Buckingham parameters for Sn−O and O−O interactions have been kept the same for bulk and slab calculations. Because of this, the agreement between the force field and ab initio geometry and Sn−O bond stretching vibrations in small clusters is not fine but acceptable (see Tables 10 and 11). After the force-field parameters are derived for water−surface interactions, another hydroxide complex $Sn_2(OH)_8(H_2O)_2$ with Sn in octahedral coordination was used to check the applicability of the derived parameters. The comparison of the VASP and force-field optimized structures of $Sn_2(OH)_8(H_2O)_2$ shows (Figure 2) a good agreement in both the bond lengths and angles.

4. Determination of Force Field Parameters for Water−Surface Interactions. The SPC/E model[19] of water was used in all our force field calculations. The SPC/E force field for H_2O is rigid, and this fact introduces some inconvenience into the force field calculations when the structure and parameter optimizations are needed. Hence, we have applied the previously used approach[7] for internal degrees of freedom of the water molecule. However, a Morse term for O−H bonding interactions was replaced by a harmonic term. Harmonic approximation has also been used for angle-bending potential. The parameters of the harmonic potentials have been fitted to reproduce the SPC/E geometry of water molecule and vibrational frequencies[7] calculated using the B3LYP method. The resulting parameters are given in Table 9. Though properties of the water molecule using harmonic potentials are practically the same as those previously derived using the Morse term for O−H bond stretching, the harmonic approximation is more durable in the statistical mechanic simulations.

For H_2O-SnO_2 surface interactions, the Lennard-Jones form of interatomic potential was adopted. The Lennard-Jones potential was used in the SPC/E water model for intermolecular

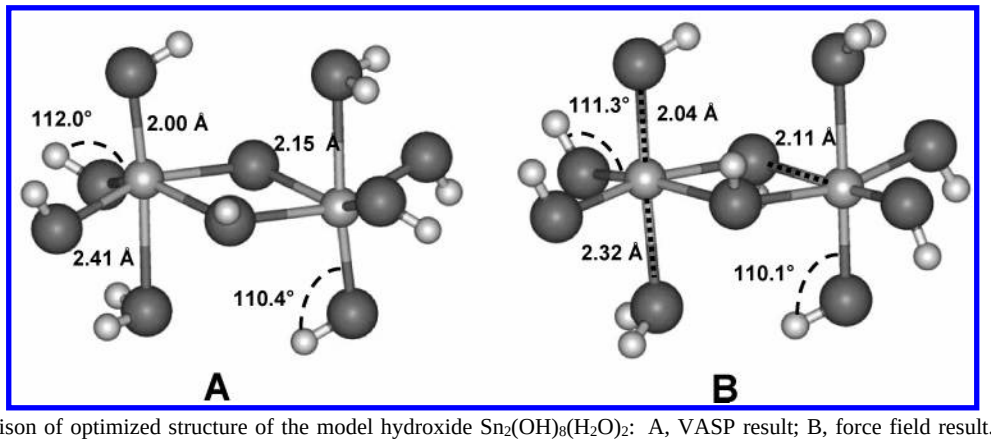

Figure 2. Comparison of optimized structure of the model hydroxide $Sn_2(OH)_8(H_2O)_2$: A, VASP result; B, force field result.

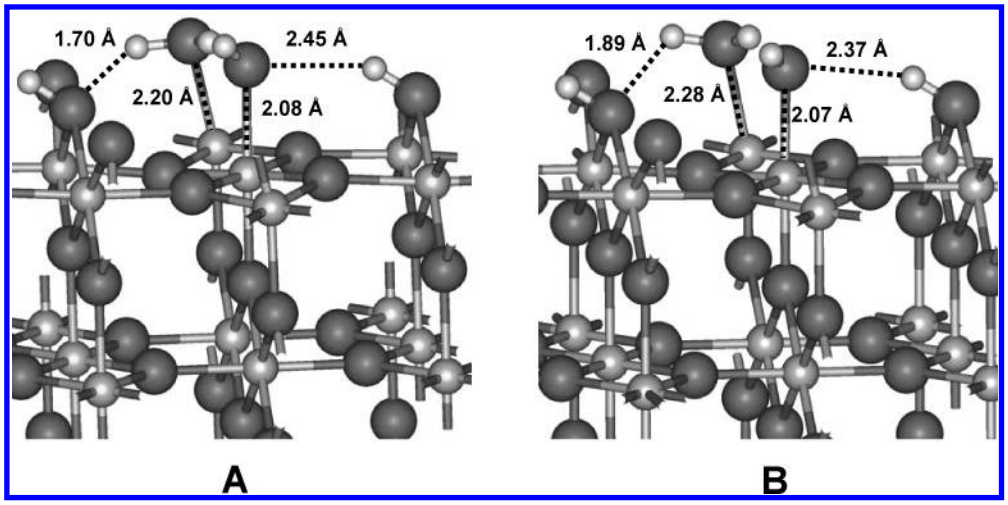

Figure 3. Comparison of optimized structure of the mixed dissociatively and associatively hydroxylated SnO_2 (110) surface (monolayer coverage): A, VASP result; B, force field result.

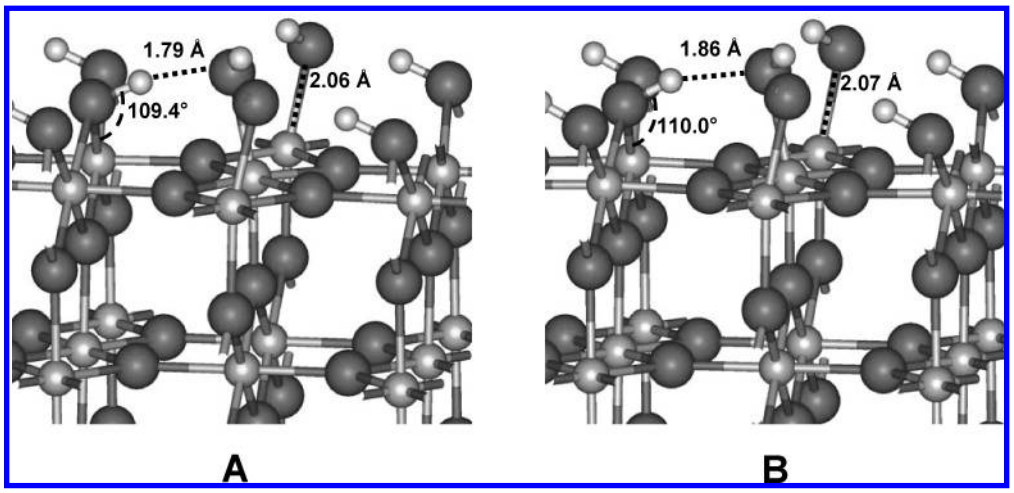

Figure 4. Comparison of optimized structure of the dissociatively hydroxylated SnO_2 (110) surface (monolayer coverage): A, VASP result; B, force field result.

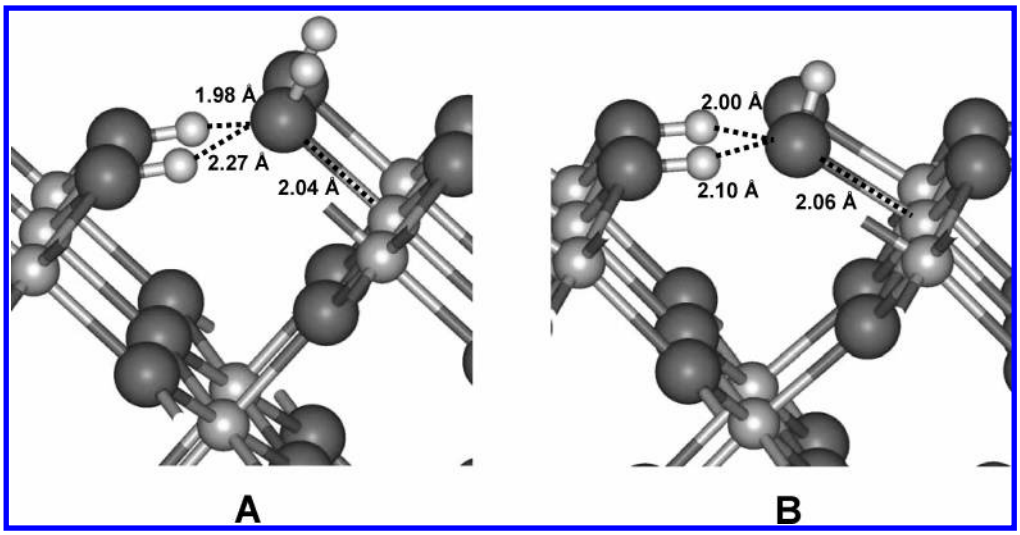

Figure 5. Comparison of optimized structure of the dissociatively hydroxylated SnO_2 (100) surface (monolayer coverage): A, VASP result; B, force field result.

interactions, and it has also been applied to ion−water and ion−surface interactions in a previous MD study[8] of an electric double layer near the rutile surface. Because there is only one adjustable parameter A_{ij} (C_{ij} can be estimated theoretically), Lennard-Jones potentials are more suitable for fitting to ab initio results. In our force field scheme, three parameters, $A_{Sn-O_{water}}$, $A_{O-O_{water}}$, and $A_{O_h-O_{water}}$ (O_h = protonated bridging or terminal oxygen) were adjusted to better reproduce the surface−water interactions.

Two systems were chosen for obtaining these values. The first one was obtained by restricted relaxation of the 1×1 SnO_2 (110) surface unit cell with one (on each side of the slab)

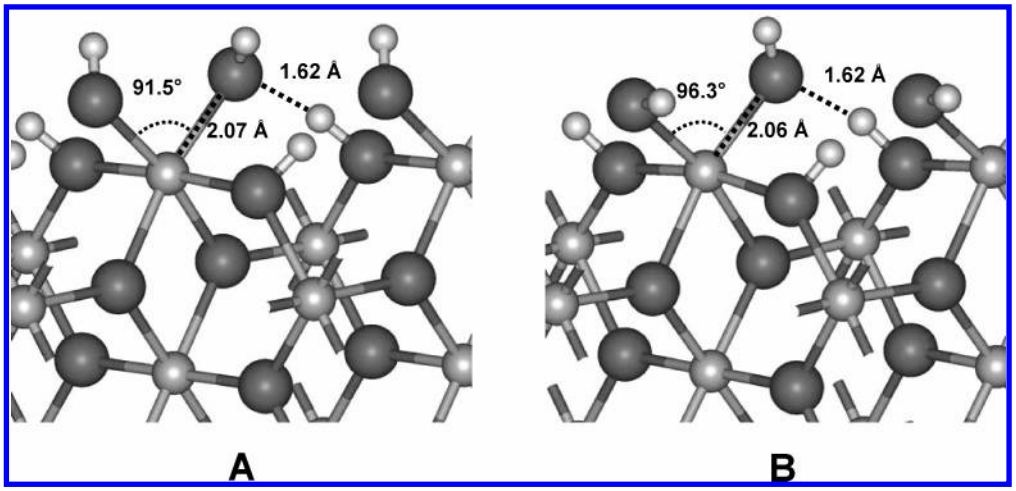

Figure 6. Comparison of optimized structure of the dissociatively hydroxylated SnO_2 (001) surface (monolayer coverage): A, VASP result; B, force field result.

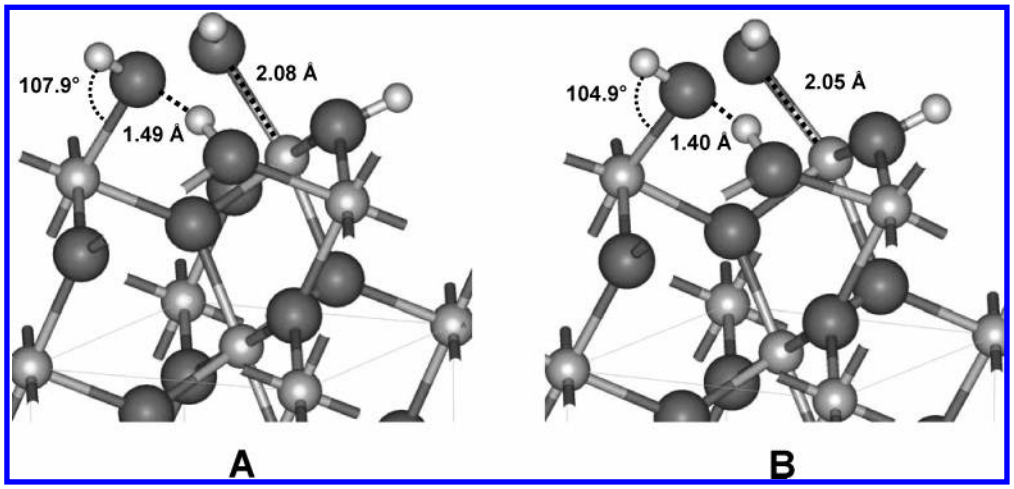

Figure 7. Comparison of optimized structure of the dissociatively hydroxylated SnO_2 (101) surface (monolayer coverage): A, VASP result; B, force field result.

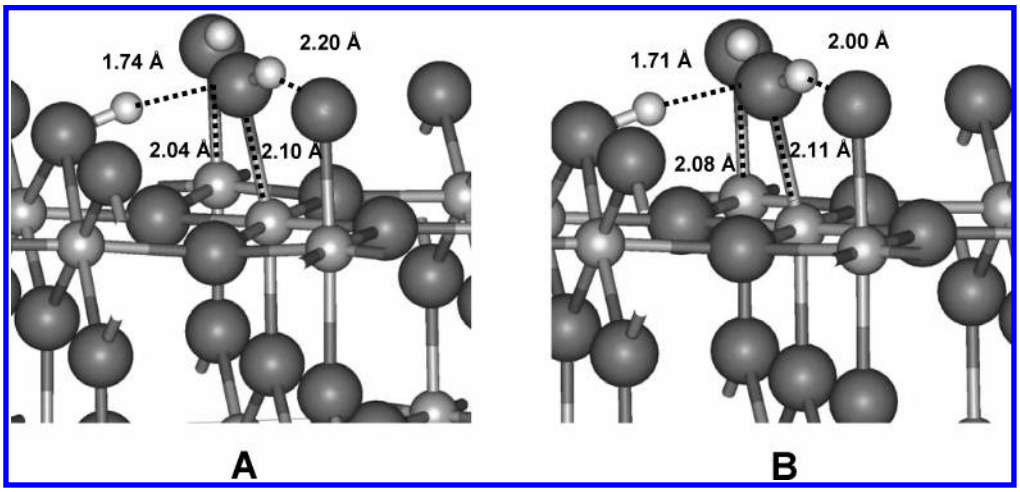

Figure 8. Optimized structure of the negatively charged hydroxylated SnO_2 (110) surface (monolayer coverage) using the neutralizing background: A, VASP result; B, force field result.

associatively adsorbed water molecule. During the VASP optimization process, the positions of the central layer atoms, the 6-fold tin Sn_{6f} on the surface, and all O atoms connected to it in the $(1\bar{1}0)$ plane were fixed. These additional restrictions were needed to prevent the spontaneous water dissociation on SnO_2 surface which was found in the case of full relaxation (Figure 3). Initial coordinates for the SnO_2 slab system were taken from the relaxed bare surface (Figure 1). The second system used was the mixed case of water adsorption on the SnO_2 (110) surface (Figure 3) which was obtained by VASP optimization beginning from the associatively adsorbed initial state. Removing of one water molecule (per slab side) leads to a system with the half-monolayer of dissociatively adsorbed water. We also have performed the optimization of this system to provide the estimation of the stepwise adsorption energy for the hydroxylated (110) surface. Both water-containing systems

TABLE 12: VASP Atomic Charges (*e*) Used in the Force-Field Calculations of the Hydroxylated SnO_2 Slab Models for the Dissociatively Adsorbed Monolayer

	face index			
atom[a]	110	100	001	101
Sn_{5f}/Sn_{4f}, (former) 5- or 4-fold tin	2.052	2.050	2.093	2.086
Sn_{6f}, 6-fold tin near the surface	2.046	2.065	2.099	2.096
Sn_m, 6-fold tin in the middle layer	2.051[b]	2.066	2.124	
O_{term}, oxygen in terminal hydroxyl	−0.945	−0.967	−0.956	−1.009
O_{br}, (protonated) bridging oxygen	−1.011	−1.055	−1.100	−1.071
O_s, 3-fold surface oxygen	−1.040	−1.010		−1.001
O_{u5f}/O_{u4f}, oxygen underneath Sn_{5f} or Sn_{4f}	−0.964	−0.989	−0.961	−0.976
O_{u6f}, oxygen underneath Sn_{6f}	−1.004	−1.000		
O_m, oxygen in the middle layer	−1.044	−0.994	−0.990	
H_{term}, hydrogen in terminal hydroxyl	0.422	0.410	0.407	0.425
H_{br}, hydrogen in bridging hydroxyl	0.476	0.457	0.477	0.498

[a] See Tables 3−6 and Figure 1 in the text of the paper for atomic notations. [b] Averaged value.

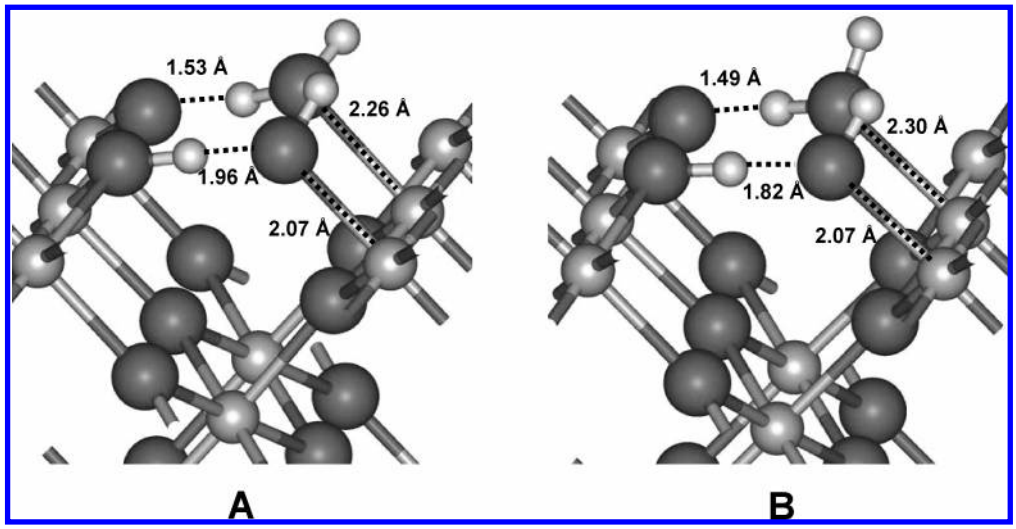

Figure 9. Comparison of mixed adsorption on SnO_2 (100) surface (monolayer coverage): A, VASP result; B, force field result.

were treated in a single fitting procedure using "RELAX" keyword within the GULP.[34] The corresponding ab initio adsorption energies (−99.6 kJ/mol for the first system, and −133.5 kJ/mol for the second) have been used to estimate the desirable force-field total energy which was accounted for in the fitting procedure. The final values of parameters for H_2O-SnO_2 surface interactions are included in Table 9. The resulting force-field structure is compared in Figure 3 to the ab initio result. The adsorption energies per molecular H_2O obtained by our force field with the final set of parameters are −103.4 kJ/mol for the first system and −138.6 kJ/mol for the second.

5. Testing the Force Field Accuracy. Application of the resulting parameters to different dissociatively hydroxylated SnO_2 surfaces is illustrated in Figures 4−7. To provide this comparison, we performed VASP calculations of the relaxed (110), (100), (001), and (101) SnO_2 surfaces covered by a monolayer of dissociatively adsorbed water molecules. We define as the monolayer such coverage when the water molecules saturate all vacant coordination places of the surface Sn up to the total coordination number 6. Inversion symmetry (space group $P\bar{1}$) was imposed on all systems containing water molecules. We used the same computational procedure as for the bare surface slabs. All these structures have been obtained via the VASP optimization starting with the dissociatively adsorbed initial state except for the case of the (101) surface where two (per side) initially associated H_2O molecules spontaneously dissociated. It should be emphasized that no additional adjustment (using the ab initio results for hydroxylated surfaces) of empirical parameters for the hydroxyl groups has been made. Nevertheless, our force field reproduces well the lengths and directions of H bonds between hydroxyls on the surfaces of the different crystallographic indexes (see Figures 4−7).

For example, the distances $(O_{br})H-O_{term}$ are only slightly overestimated on dissociatively hydroxylated (110) surface (force field, 1.86 Å; ab initio, 1.79 Å), and slightly underestimated on (101) surface (force field, 1.40 Å; ab initio, 1.49 Å). In the case of (101) surface, both DFT and force field calculations show the formation of the extremely short H bonds between bridging and terminal hydroxyls (Figure 7). For (100) (Figure 5) and (001) (Figure 6) surfaces, the deviations between force-field and VASP results are even lower, except perhaps the exact orientation of hydroxyl groups. Also, our force field reconstructs the charged (110) surface model which was produced by removing one of the bridging protons from dissociatively hydroxylated surface. The charged systems have been calculated using the neutralizing background. The surface structure does not change significantly from a neutral surface to this charged surface (Figure 8). However, this example shows that parameters of our force field are transferable for description of the nonneutral systems.

As in the case for the bare relaxed SnO_2 surfaces, the force field parametrization reproduces the ab initio atomic relaxation results fairly accurately. From our point of view, this success, as well as the parameter transferability, is mainly due to advances of the adopted scheme for extracting the atomic charges from VASP results. The atomic charges used in the

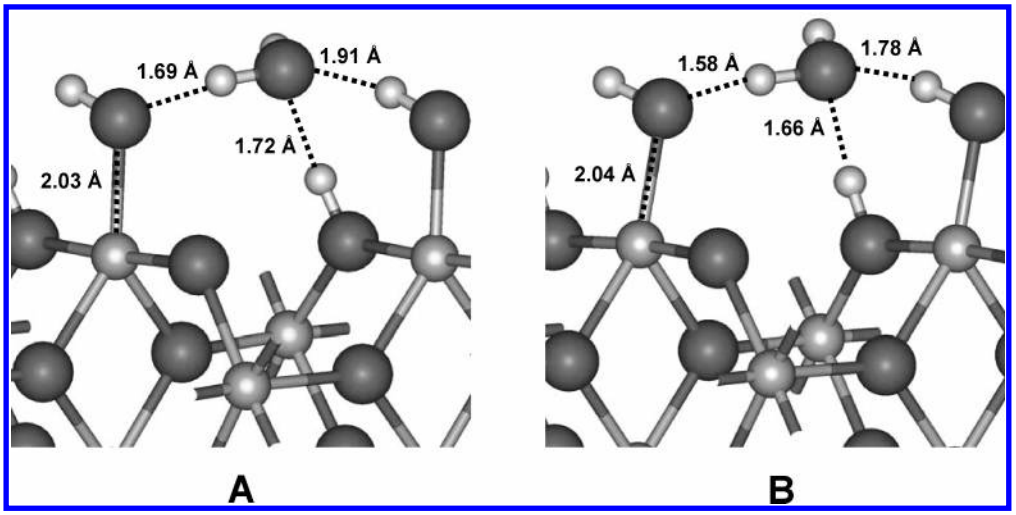

Figure 10. Comparison of mixed adsorption on SnO_2 (001) surface: A, VASP result; B, force field result.

TABLE 13: Ab Initio Adsorption Energies per Water Molecule for Different Configurations of H_2O Monolayer on SnO_2 Surfaces (kJ/mol)

face index	surface cell[a]	no. of water molecules per one side of slab	associative adsorption	mixed adsorption	dissociative adsorption
110	2 × 1	2	−113.1[b]	−142.9[c]	−145.9
	1 × 1	1	−75.3 (ref 9)[d]		−134.1 (ref 9)[d]
	2 × 1	2	unstable (ref 10)	−165.9 (ref 10)	−170.8 (ref 10)
	2 × 2	4	unstable (ref 11)	−140.9 (ref 11)	−165.0 (ref 11)
100	1 × 1	1	−95.9	−98.6[e]	−106.4
001	1 × 1	2	unstable	−117.8	−136.9
101	1 × 1	2	unstable	unstable	−146.2

[a] See Table 2 for slab dimensions. [b] Calculated with restricted relaxation (see text). [c] Stepwise adsorption energies: −152.3 kJ/mol, for the first (per side) dissociatively adsorbed molecule; −133.5 kJ/mol, for the second, associatively adsorbed water molecule. [d] Obtained in ref 9 by the partial geometry optimization. [e] Doublet (2 × 1) surface unit cell has been used.

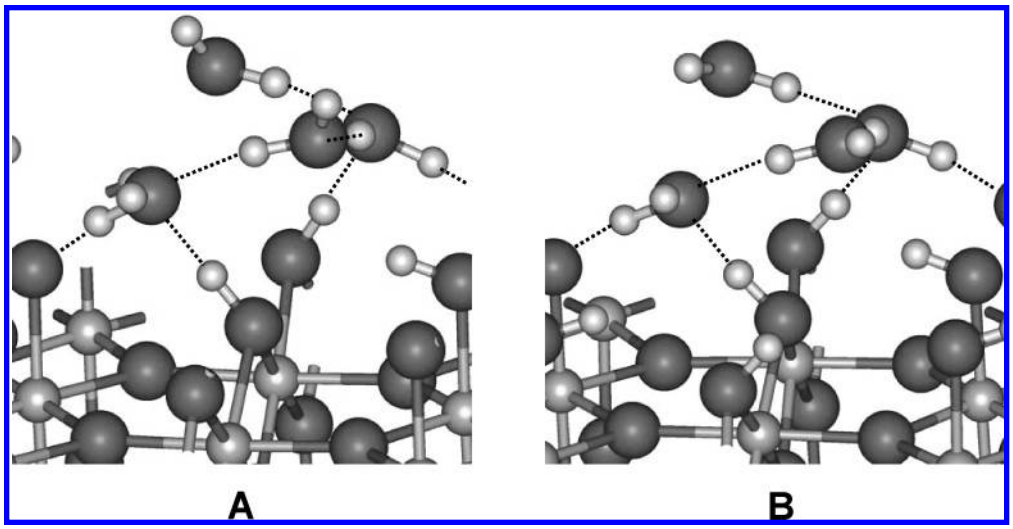

Figure 11. Structure of the second adsorption layer above the dissociatively adsorbed first layer on (110) SnO_2 surface: A, VASP result; B, force field result. The H bonds between surface hydroxyls and water molecules are dotted.

force-field calculations of hydroxylated surfaces are given in Table 12.

The (100) face of SnO_2 seems to be the only one where the fully associative adsorption may be possible. At least, an adsorbed H_2O molecule (one per side in a 1 × 1 surface unit cell) did not dissociate during the ab initio optimization. To check the possibility of the mixed associative−dissociative adsorption on the (100) surface, we investigated the corresponding initial state using the doubled 2 × 1 unit cell (Figure 9). The final structure has a lower energy than the purely molecular adsorption. In Figure 10, we compare the optimized structure of a hydroxylated (001) surface of SnO_2 obtained using VASP and the derived force field for the mixed monolayer adsorption. Ab initio structure has been obtained starting with the associatively adsorbed initial state, but as in the case of the (110) surface, one (per side) water molecule spontaneously dissociated. Our attempt to obtain the stable structure with the associatively adsorbed water molecules on (101) surface failed: on the monolayer-covered (101) SnO_2 surface, the H_2O molecules dissociated completely.

Adsorption energies obtained via ab initio calculations are given in Table 13 for all considered monolayer structures. It

can be seen that the dissociative adsorption is more favorable for all SnO_2 faces. Mixed adsorption energy takes the intermediate position between the associative and dissociative values, but for the (110) face it is very close to the dissociative figure. From our ab initio results, we can conclude that water may exist in molecular form on the (110) and (100) surfaces, while on (001) and (101) surfaces this is improbable. The largest (and almost equal) water adsorption energies are attained on the (110) and (101) surfaces.

Note that we could not compare the force-field energies of associative and dissociative adsorption because of variations of the chemical bonds and the different atomic charges used in the regarded systems. However, we can estimate the gain of energy in one case of the associative adsorption where the mentioned parameters do not change. For the (100) surface, the force field gives −124.8 kJ/mol per one water molecule which is than greater the ab initio value, −95.8 kJ/mol, but it is in correct order relative to stepwise adsorption energy on the (110) surface (−138.6 kJ/mol).

In the case of the (110) surface, we investigated the water adsorption beyond the monolayer. One can suppose that the number of possible configurations rises considerably when one or several water molecules are added to molecules composing the monolayer on the (110) surface. Consequently, investigation of the adsorbate structure beyond the monolayer is a complicated task for static ab initio calculations. However, one probable low-energy structure can be indicated when four extra molecules are placed above the monolayer of dissociatively adsorbed water molecules on the (110) SnO_2 surface (Figure 11). The pair of additional molecules can organize the "bridges" between the terminal and bridging hydroxyls

$$\equiv Sn_2O_{br}-H\cdots\overset{H}{O}-H\cdots\overset{H}{O}_{term}-Sn\equiv$$

The other two H_2O molecules can connect the previous two in neighboring cells. Our force field predicts this structure to be the most stable arrangement of the second adsorption layer on (110) surface. We have used the force-field-obtained structure as an initial guess to VASP optimization. On comparison of the ab initio and force field results in Figure 11, it can be seen that agreement is good. The energy gain per H_2O molecule in the formation of the second layer is −48.2 and −70.8 kJ/mol for VASP and force field results, respectively. The overestimation of this value by the force field may be due to exceeding the SPC/E water−water interaction energy, −31.3 kJ/mol, relative to the ab initio value, −22.3 kJ/mol. Hence, the energy gain in the second layer approximately corresponds to the formation of two H bonds per water molecule.

Summary

With DFT theory the various models of relaxed in vacuo SnO_2 surfaces have been calculated. Adsorption of water molecules on faces with different low crystallographic indexes has been considered. The dissociative water adsorption was found to be the most favorable for all considered SnO_2 faces. The mixed adsorption structure may be stable on (110) and (100) surfaces, whereas on (001) and (101) the water molecules in the first layer are most probably completely dissociated.

On the basis of the VASP results an empirical force field was derived that can correctly predict the surface relaxations and water−surface interactions. The H bond lengths between the water molecules and surface hydroxyls and water−surface distances produced by force field deviate from the ab initio values less than 0.15 Å. The proposed force field can be used in the molecular dynamic simulations of the boundary between the tin dioxide and aqueous solutions.

Acknowledgment. This research was supported by the U.S. Department of Energy, Office of Basic Energy Sciences, Division of Chemical Sciences, Geosciences and Biosciences, under the project "Nanoscale Complexity at the Oxide-Water Interface" and by NSF Grant EAR-0073722 "Adsorption of cations on mineral−aqueous solution interfaces at elevated temperatures". Computation was supported in part by the Materials Simulation Center, a Penn-State MRSEC and MRI facility, and the Center for Environmental Kinetics Analysis, an NSF/DOE Environmental Molecular Sciences Institute.

References and Notes

(1) Whittaker M., Floyd C. D., Brown P, Gearing A. J. *Chem. Rev.* **1999**, *99*, 2735−2776.

(2) Fedkin, M. V.; Zhou, X. Y.; Kubicki, J. D.; Bandura, A. V.; Lvov, S. N.; Wesolowski, D. J.; Machesky, M. L. *Langmuir* **2003**, *19*, 3797−3804.

(3) Zhang, Z.; Fenter, P.; Cheng, L.; Sturchio, N. C.; Bedzyk, M. J.; Pøedota, M.; Bandura, A. V.; Kubicki, J. D.; Lvov, S. N.; Cummings, P. T.; Chialvo, A. A.; Ridley, M. K.; Bénézeth, P.; Anovitz, L.; Palmer, D. A.; Machesky, M. L.; Wesolowski, D. J. *Langmuir* **2004**, *20*, 4954−4969.

(4) Bandura, A. V.; Sykes, D. G.; Shapovalov, V.; Troung, T. N.; Kubicki, J. D.; Evarestov, R. A. *J. Phys. Chem. B* **2004**, *108*, 7844−7853.

(5) Fitts, J. P.; Machesky, M. L.; Wesolowski, D. J.; Shang, X.; Kubicki, J. D.; Flynn, G. W.; Heinz, T. F.; Eisenthal, K. B. *Chem. Phys. Lett.*, in press.

(6) Sverjensky, D. A. *Nature* **1993**, *364*, 776−780.

(7) Bandura, A. V.; Kubicki, J. D. *J. Phys. Chem. B* **2003**, *107*, 11072−11081.

(8) Predota, M.; Bandura, A. V.; Cummings, P. T.; Kubicki, J. D.; Wesolowski, D. J.; Chialvo, A. A.; Machesky, M. L. *J. Phys. Chem. B* **2004**, *108*, 12049−12060.

(9) Goniakowski, J.; Gillan, M. J. *Surf. Sci.* **1996**, *350*, 145−158.

(10) Lindan, P. J. D. *Chem. Phys. Lett.* **2000**, *328*, 325−329.

(11) Bates, S. P. *Surf. Sci.* **2002**, *512*, 29−36.

(12) Matsui, M.; Akaogi, M. *Mol. Simul.* **1991**, *6*, 239−245.

(13) Urusov, V. S.; Eremin, N. N. *Phys. Chem. Miner.* **1997**, *24*, 374−383.

(14) Minervini, L.; Grimes, R. W.; Sickafus, K. E. *J. Am. Ceram. Soc.* **2000**, *83*, 1873−1878.

(15) Woodley, S. M.; Battle, P. D.; Gale, J. D.; Catlow, C. R. A. *Phys. Chem. Chem. Phys.* **1999**, *1*, 2535−2542.

(16) Lewis, G. V.; Catlow, C. R. A. *J. Phys. C*: *Solid State Phys.* **1985**, *18*, 1149−1161.

(17) Freeman, C. M.; Catlow, C. R. A. *J. Solid State Chem.* **1990**, *85*, 65−73.

(18) Dick, B. G.; Overhauser, A. W. *Phys. Rev.* **1958**, *112*, 90−103.

(19) Berendsen, H. J. C.; Grigera, J. R.; Straatsma, T. P. *J. Phys. Chem.* **1987**, *91* (24), 6269−6271.

(20) Kresse, G.; Furthmüller, J. *Phys. Rev. B* **1996**, *54*, 11169−11186.

(21) Kresse, G.; Furthmüller, J. *Vasp the Guide*. Institut für Materialphysik, Universität Wien: Vienna, Austria, 2003.

(22) Kresse, G.; Joubert, J. *Phys. Rev. B* **1999**, *59*, 1758−1775.

(23) Blöchl, P. E. *Phys. Rev. B* **1994**, *50*, 17953−17979.

(24) Perdew, J. P.; Burke, K.; Ernzerhof M. *Phys. Rev. Lett.* **1996**, *77*, 3865−3868.

(25) Bolzan, A. A.; Fong, C.; Kennedy, B. J.; Howard, C. J. *Acta Crystallogr.* **1997**, *53*, 373−380.

(26) Monkhorst, H. J.; Pack, J. D. *Phys. Rev.* **1976**, *13*, 5188−5192.

(27) Frisch, M. J.; Trucks, G. W.; Schlegel, H. B.; Scuseria, G. E.; Robb, M. A.; Cheeseman, J. R.; Montgomery, J. A., Jr.; Vreven, T.; Kudin, K. N.; Burant, J. C.; Millam, J. M.; Iyengar, S. S.; Tomasi, J.; Barone, V.; Mennucci, B.; Cossi, M.; Scalmani, G.; Rega, N.; Petersson, G. A.; Nakatsuji, H.; Hada, M.; Ehara, M.; Toyota, K.; Fukuda, R.; Hasegawa, J.; Ishida, M.; Nakajima, T.; Honda, Y.; Kitao, O.; Nakai, H.; Klene, M.; Li, X.; Knox, J. E.; Hratchian, H. P.; Cross, J. B.; Bakken, V.; Adamo, C.; Jaramillo, J.; Gomperts, R.; Stratmann, R. E.; Yazyev, O.; Austin, A. J.; Cammi, R.; Pomelli, C.; Ochterski, J. W.; Ayala, P. Y.; Morokuma, K.; Voth, G. A.; Salvador, P.; Dannenberg, J. J.; Zakrzewski, V. G.; Dapprich, S.; Daniels, A. D.; Strain, M. C.; Farkas, O.; Malick, D. K.; Rabuck, A. D.; Raghavachari, K.; Foresman, J. B.; Ortiz, J. V.; Cui, Q.; Baboul, A. G.; Clifford, S.; Cioslowski, J.; Stefanov, B. B.; Liu, G.; Liashenko, A.; Piskorz, P.; Komaromi, I.; Martin, R. L.; Fox, D. J.; Keith, T.; Al-Laham, M. A.; Peng, C. Y.; Nanayakkara, A.; Challacombe, M.; Gill, P. M. W.; Johnson, B.; Chen, W.; Wong, M. W.; Gonzalez, C.; Pople, J. A. *Gaussian 03*, Revision C.02; Gaussian, Inc.: Wallingford, CT, 2004.

(28) Breneman, C. M.; Wiberg, K. B. *J. Comput. Chem.* **1990**, *11*, 361−373.
(29) Peterson, K. A. *J. Chem. Phys.* **2003**, *119*, 11099−11112.
(30) Hiemstra, T.; Yong, H.; Van Riemsdijk, W. H. *Langmuir* **1999**, *15*, 5942−5955.
(31) Oviedo, J.; Gillan, M. J. *Surf. Sci.* **2000**, *463*, 93−101.
(32) Perdew, J. P. Unified Theory of Exchange and Correlation beyond the Local Density Approximation. In *Electronic structure of solids ′91*; Ziesche, P., Eschrig, H., Eds.; Akademic Verlag: Berlin, 1991; pp 11−20.
(33) Vanderbilt, D. *Phys. Rev. B* **1990**, *41*, 7892−7895.
(34) Gale, J. D. *J. Chem. Soc., Faraday Trans* **1997**, *93* 629−637.
(35) Chang, E.; Graham, E. K. *J. Geophys. Res.* **1975**, *80*, 2595−2599.
(36) Fowler, P. W.; Harding, J. H.; Pyper, N. C. *J. Phys.*: *Condens. Matter* **1994**, *6*, 10593−10606.
(37) Dimitrov, V.; Komatsu, T. *J. Solid State Chem.* **2002**, *163*, 100−112.
(38) Parlinskia, K.; Kawazoe, Y. *Eur. Phys. J. B* **2000**, *13*, 679−683.
(39) Katiyar, R. S.; Dawson, P.; Hargreave, M. M.; Wilkinson, G. R. *J. Phys. C*: *Solid State Phys.* **1971**, *4*, 2421−2431.
(40) Peercy, P. S.; Morosin, B. *Phys. Rev. B*: *Condens. Matter* **1973**, *7*, 2779−2786.
(41) Hay, P. J.; Wadt, W. R. *J. Chem. Phys*. **1985**, *82*, 270−283.
(42) Check, C. E.; Faust, T. O.; Bailey, J. M.; Wright, B. J.; Gilbert, T. M.; Sunderlin, L. S. *J. Phys. Chem. A* **2001**, *105*, 8111−8116.
(43) Martin, J. M. L.; Sundermann, A. *J. Chem. Phys.* **2001**, *114*, 3408−3420.
(44) Becke, A. D. *J. Chem. Phys.* **1993**, *98*, 5648−5652.
(45) Lee, C.; Yang, W.; Parr, R. *Phys. Rev. B* **1988**, *37*, 785−789.